Available online at www.sciencedirect.com
SCIENCE DIRECT®
Thermochimica Acta 419 (2004) 173–179
thermochimica acta
www.elsevier.com/locate/tca

Physicochemical characterization of the decomposition course of hydrated ytterbium nitrate: thermoanalytical studies

Basma A.A. Balboul*

Chemistry Department, Faculty of Science, Minia University, El-Minia 61519, Egypt

Received 14 August 2003; received in revised form 12 December 2003; accepted 13 December 2003

Available online 14 April 2004

Abstract

$Yb(NO_3)_3{\cdot}6H_2O$ was used as a parent compound for the formation of Yb_2O_3 at up to 800 °C in atmosphere of air. Thermal processes occurring during the decomposition course were monitored by means of differential thermal analysis (DTA), thermogravimetry (TG), and the gaseous decomposition products were identified by mass spectrometry (GC–MS). The intermediates and final solid products were characterized by IR-spectroscopy, X-ray diffraction (XRD) and scanning electron microscopy (SEM). The results showed that, $Yb(NO_3)_3{\cdot}6H_2O$ decomposes completely through 11 endothermic mass loss processes. The dehydration occurs through the first six steps at 95, 145, 165, 175 and 200 °C, forming crystalline nitrate $Yb(NO_3)_3$, which decomposes to $YbO_{0.5}(NO_3)_2$ at 250 °C. The latter, decomposes to non-stoichiometric unstable intermediate $YbO_{0.75}(NO_3)_{1.5}$ at 335 °C, which decompose immediately to a stable and crystalline $YbONO_3$ at 365 °C, then to a non-stoichiometric unstable intermediate $Yb(O)_{1.25}(NO_3)_{0.5}$ at 470 °C. Finally, Yb_2O_3 was formed at 510 °C. The decomposition course and surface morphology were supported and followed by SEM and textural studies (S_{BET}).The final product Yb_2O_3 at 600 °C has a large irregular sheet shaped particles containing a large pores, voids and cracks and has $S_{BET} = 45\,m^2/g$. The gaseous decomposition products are water vapor, nitric acid and nitrogen oxides (NO, NO_2 and N_2O_5). The activation energy (ΔE in kJ/mol) was calculated non-isothermally for each thermal processes.

Keywords: Yb-nitrate; Yb-oxide; Decomposition; Formation; DTA; TG; XRD; GC–MS; S_{BET}; SEM

1. Introduction

The sesquioxide, Yb_2O_3, has a cubic structure below 1870 °C, at higher temperatures it exists as monoclinic and hexagonal phase [1]. The Yb_2O_3 with cubic structure has been used as catalyst in the dehydration of alkan-2-ols to alk-1-enes and for the oxidative coupling of methane (i.e. a petrochemical industrial catalyst [2,3]). Yb_2O_3 is a basic oxide whose basicity and catalytic properties are dependent on the method of preparation and pretreatment [3]. There is a little information available on literature about the decomposition course of Yb-salts compared to other rare earth metal salts.

Several studies [4–11] and a review article [12] have been published concerning with the thermal decomposition of rare earth metal salts. It was reported [12] that, rare earth metal oxides obtained from nitrate or acetate precursors leads to higher surface area compared with those obtained from oxalate precursors. Patil et al. [4] reported that, the formation of M_2O_3 from rare earth nitrates takes place via the oxy-nitrate ($MONO_3$). They also reported the possible formation of anhydrous nitrate, while Wendlandt and Bear [5] stated that the anhydrous nitrates are unstable. Stewart and Wendlandt [6] studied the decomposition of $La(NO_3)_3{\cdot}6H_2O$. They reported that, the dehydration takes place at 105 °C to give $La(NO_3)_3{\cdot}3H_2O$, which decomposes at 200 °C to form a basic nitrate; and at 500 °C, La_2O_3 was the final product. Recently, the decomposition of $Y(NO_3)_3{\cdot}5H_2O$, was studied [7]. It was reported that a thermally stable monohydrate was formed. Also a mixture of $Y(NO_3)_3$ and $Y(OH)(NO_3)_2$ were obtained at 270 °C; and $YONO_3$ was detected by XRD as crystalline phase at 325 °C. Y_2O_3 was the final product at 500 °C. The texture analysis by nitrogen adsorption method [8], revealed that Y_2O_3 obtained from $Y(NO_3)_3{\cdot}5H_2O$ at 500 °C has a higher surface area ($S_{BET} = 58\,m^2/g$) compared with that obtained at 700 °C ($S_{BET} = 20\,m^2/g$).

* Tel.: +20-86-345231; fax: +20-86-342601.
E-mail address: bsma64@yahoo.com (B.A.A. Balboul).

0040-6031/$ – see front matter © 2004 Elsevier B.V. All rights reserved.
doi:10.1016/j.tca.2003.12.029

They attribute the lower surface area as results of sintering. Hussein et al. [9,10] have studied the decomposition course of $Th(NO_3)_4{\cdot}5H_2O$ [12] and $Dy(NO_3)_3{\cdot}6H_2O$ [10] in air by TG, DTA, IR, XRD and SEM. They reported that, the anhydrous nitrates are thermally unstable and the decompositions gave ThO_2 at 300 °C and Dy_2O_3 at 600 °C, respectively. Different intermediates of non-stoichiometric oxy-nitrates were also detected. The $DyONO_3$ is crystalline and thermally stable, compared to $ThO(NO_3)_2$ which is unstable and amorphous. Basma and Balboul [13] studied the decomposition course of $Ho(NO_3)_3{\cdot}5H_2O$ in air by TG, DTA, IR, XRD and SEM. It was reported that, the anhydrous nitrates are thermally unstable and the decomposition gave Ho_2O_3 at 560 °C. Different intermediates of non-stoichiometric oxy-nitrates were also detected. The $HoONO_3$ is crystalline and thermally stable.

The present investigation is intended to characterize the thermal decomposition course of $Yb(NO_3)_3{\cdot}6H_2O$ to the onset of Yb_2O_3 formation by means of thermogravimetric (TG) and differential thermal analysis (DTA). The volatile decomposition products were analyzed by means of gas chromatography–mass spectrometry (GC–MS), while the solid reaction products were characterized by X-ray diffraction (XRD). Scanning electron microscopy (SEM) was used to characterize the progressive changes in the morphology of the nitrate samples as they convert to the oxide. The oxide formed at 600 °C was subjected to surface area measurements by N_2 adsorption. The activation energy (ΔE in kJ/mol) was determined non-isothermally for the decomposition processes involved.

2. Experimental

2.1. Materials

$Yb(NO_3)_3{\cdot}6H_2O$, abbreviated as YbNit, was 99.9% pure (Aldrich, USA). It was used as received. Its calcination products were obtained by heating at various temperatures (200–600 °C) for 1 h in static air. The calcination temperatures were chosen on bases of the thermal analysis results. Prior to analysis, the calcination products were kept dry over Silica Gel. For simplicity, these products are donated in the text by YbNit, followed by the calcination temperatures. Thus, YbNit-400 indicates decomposition products of YbNit at 400 °C for 1 h. The abbreviation ML stands for mass loss.

2.2. Thermal analysis

Thermal analysis were performed using DuPont 9900, Model DTA 951-TG 910 (USA). Thermogravimetry and differential thermal analysis curves were recorded up to 700 °C at different heating rates (5–50 °C/min), in static air atmosphere. Equal weights of the test sample (ca. 15 mg) were used in TG measurements. Highly sintered α-Al_2O_3 was the reference material for the DTA measurements.

From the thermoanalytical data, the temperature (T_{max}) obtained from the DTA curve, were determined as a function of the heating rate (θ) applied. The activation energy (ΔE in kJ/mol) was then calculated for each process using Kissinger equation [14].

2.3. Gas–mass spectrometry

All the gas–mass spectra of the volatile decomposition products were recorded with a Hewlett Packard (HP-5890 series II) gas chromatograph equipped with a 5971 mass selective detector. An HP-vectra Q5/165F data station was used for acquisition and processing of the spectra. Also the data station was equipped with ATLAS software for comparison and identification purposes.

The spectra of the gaseous products of YbNit were taken using a sample cell Tekmar 5 ml frit sparger (Pn 14-2337-024). Some modifications were made by heating the sample area with additional coiled heater equipped with temperature controller. This makes the cell to work as a variable temperature cell.

The standard procedure for automated GC–MS were as follows: powder sample (20 mg) was heated at different temperatures (150–450 °C) for 5 min. At each temperature, the gaseous products were trapped using Tekmar LSC2000, dynamic head space concentrator. The trapped products were automatically disrobed into a HP-5890 GC, interfaced with a 5971A mass-selective detector.

The gaseous decomposition products were injected at 200 °C to the GC equipped with 60 m × 0.25 mm DP5 column, with a 2.5 μm film thickness. It is held at 50 °C for 10 min after injection, then programmed to 240 °C. The N_2 gas was used as a carrier gas at a flow rate 1.0 ml/min.

To prepare for the next experiment (decomposition temperature), the trap (LSC2000) was baked out at 250 °C for 10 min under a flow of N_2 gas.

2.4. Infrared spectroscopy

IR spectra were obtained at a resolution of 4 cm^{-1}, between 4000 and 400 cm^{-1}, using a model FT/IR 410 JASCO (Japan). IR spectra of YbNit and its solid calcination products were obtained from thin, lightly loaded (<1%) KBr-supported discs.

2.5. X-ray diffraction

XRD powder patterns were obtained using JSX-60P JEOL diffractometer equipped with Ni-filter and generates a beam of Cu Kα radiation ($\lambda = 1.5418$ Å). The operational settings for all the XRD scans are voltage: 40 kV; current: 30 mA; 2θ = range 4–60°; scanning speed = 8°/min; slit width = 0.02°. For identification purposes the relative intensities (I/I°) and the d-spacing (Å) were compared with standard diffraction patterns of the ASTM powder diffraction files [15].

2.6. Scanning electron microscopy

SEM was performed using a Shimadzu (Kyoto, Japan) electron probe microanalyzer (EPMA 8705) operated at 20 kV. Samples of YbNit and its calcination products were mounted separately on aluminum stubs, evacuated to 10^{-3} Torr and pre-coated (20 and 5 min for each of the four sides) in a sputter-coater with a thin, uniform, gold–palladium film to minimize charging in the electron beam. The applied voltage was 1.2–1.6 kV.

2.7. Nitrogen sorption measurements

The N_2 sorption isotherms were determined volumetrically at −196 °C using a micro-apparatus based on the design of Lippens et al. [16]. The test sample (YbNit-600) was out-gassed at 200 °C for 2 h under evacuation at 10^{-5} Torr.

3. Results and discussion

3.1. Characterization of thermal processes

The DTA curve (Fig. 1) shows 11 endothermic processes. The first endothermic weight invariant process indicates that the material melts at 60 °C. A direct visual observation of the physical changes taking place during the decomposition indicates that the material melts at 59 °C. Therefore, process 1 is due to melting.

3.1.1. Dehydration processes

Processes II–VI: The TG and DTA curves (Fig. 1) indicates that processes II–VI are overlapping endothermic mass losses processes, which maximize at 95, 145, 165, 175 and 200 °C, respectively. The mass losses observed of these processes (Table 1) are similar to that theoretically calculated for the release of 6 mol of water, hence the dehydration process most likely proceeds as follows:

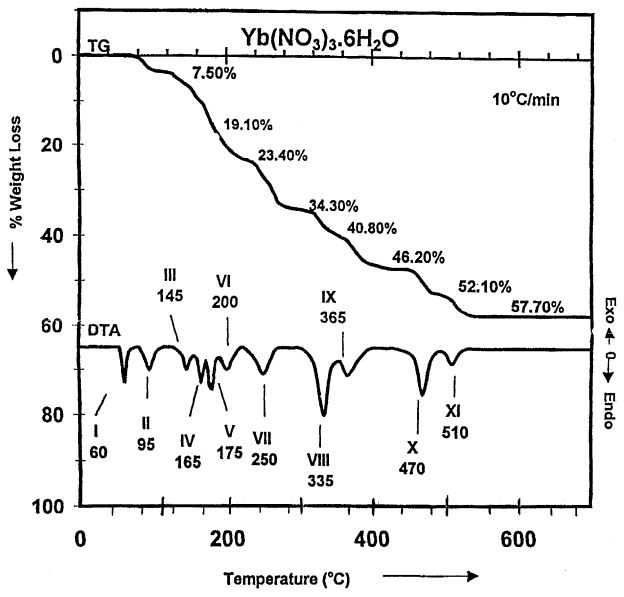

Fig. 1. TG and DTA curves recorded for YbNit at the heating rates indicated, in a dynamic (10 °C/min) atmosphere of air.

Table 1

Process (kJ/mol)	ML observed (%)	ML theoretical (%)	Composition	Activation energy
I	–	Melting	$Yb(NO_3)_3{\cdot}6H_2O$	–
II	3.85	6.85	$Yb(NO_3)_3{\cdot}5H_2O$	45
III	7.50	7.50	$Yb(NO_3)_3{\cdot}4H_2O$	41
IV	11.56	11.56	$Yb(NO_3)_3{\cdot}3H_2O$	54
V	19.27	19.27	$Yb(NO_3)_3{\cdot}1H_2O$	79
VI	23.40	23.12	$Yb(NO_3)_3$	42
VII	34.30	34.68	$YbO_{0.5}(NO_3)_2$	63
VIII	40.80	40.47	$YbO_{0.75}(NO_3)_{1.5}$	136
IX	46.20	46.25	$YbONO_3$	97
X	52.10	52.03	$YbO_{1.25}(NO_3)_{0.5}$	163
XI	57.70	57.8	Yb_2O_3	152

$$Yb(NO_3)_3 \cdot 6H_2O\ (II) \xrightarrow{95\,^\circ C} Yb(NO_3)_3 \cdot 5H_2O$$

$$Yb(NO_3)_3 \cdot 5H_2O\ (III) \xrightarrow{145\,^\circ C} Yb(NO_3)_3 \cdot 4H_2O$$

$$Yb(NO_3)_3 \cdot 4H_2O\ (IV) \xrightarrow{165\,^\circ C} Yb(NO_3)_3 \cdot 3H_2O$$

$$Yb(NO_3)_3 \cdot 3H_2O\ (V) \xrightarrow{175\,^\circ C} Yb(NO_3)_3 \cdot H_2O$$

$$Yb(NO_3)_3 \cdot H_2O\ (VI) \xrightarrow{200\,^\circ C} Yb(NO_3)_3$$

The mass spectra up to 200 °C (Fig. 2), is consistent with the TG/DTA data. Only the mass of H_2O ion (18, at a retention time of 6.5 min) and its positive radicals, $m/z = 19$, 17 and 16 [17] were detected.

The corresponding activation energy (Table 1) has values of 45 kJ/mol (II), 41 kJ/mol (III), 54 kJ/mol (IV), 79 kJ/mol (V) and 42 kJ/mol (VI). They are within the range characteristic to the dehydration processes [18,19].

3.1.2. Decomposition processes

Process VII is a strong endothermic process peaking at 250 °C. The ML loss determined (Table 1) for process VII is 34.3%, which is near to that expected 34.6% for the formation of the amorphous phase $YbO_{0.5}(NO_3)_2$.

$$Yb(NO_3)_3\ (VII) \xrightarrow{250\,^\circ C} YbO_{0.5}(NO_3)_2$$

The XRD-pattern (Fig. 3) at 300 °C indicates the presence of the anhydrous $Yb(NO_3)_3$ as a crystalline phase. The IR spectrum YbNit-300 (Fig. 4) is similar to that obtained for untreated YbNit. Except for the disappearance of bands due to water of crystallization. It displays bands at 1500, 1320, 1040 and 830 cm^{-1} due to nitrate groups of a mainly shelving bidentate structure [20,21].

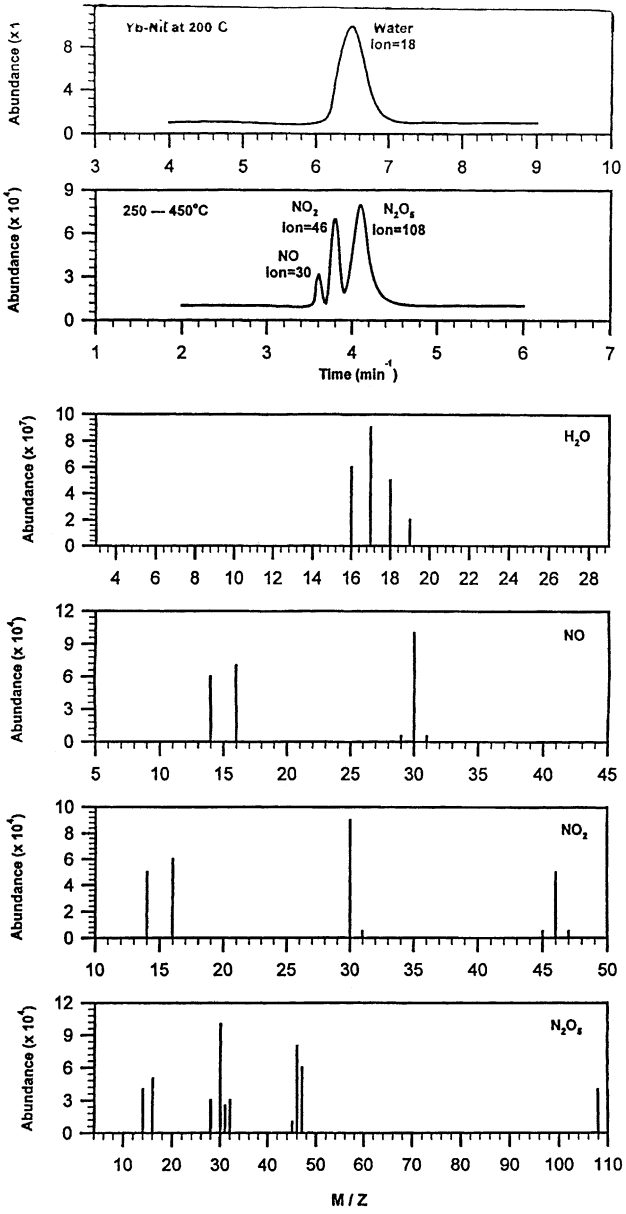

Fig. 2. Gas–mass spectra recorded from the gas surrounding a 20 mg portion of YbNit at the temperatures indicated.

The low activation energy of the first decomposition process (VII), 63 kJ/mol, indicates the unstability of the anhydrous YbNit.

Processes VIII and IX are strongly overlapped, endothermic maximized at 335 and 365 °C. The mass loss associated with each process (Table 1) was close to that equivalent to the formation of nonstiochiometric unstable form of oxynitrate $YbO_{0.75}(NO_3)_{1.5}$ and to the thermally stable intermediate $YbONO_3$, respectively.

$$YbO_{0.75}(NO_3)_2\ (VIII) \xrightarrow{335\,^{\circ}C} YbO_{0.75}(NO_3)_{1.5} + N_2O_5$$

$$YbO_{0.75}(NO_3)_{1.5}\ (IX) \xrightarrow{365\,^{\circ}C} YbONO_3 + N_2O_5$$

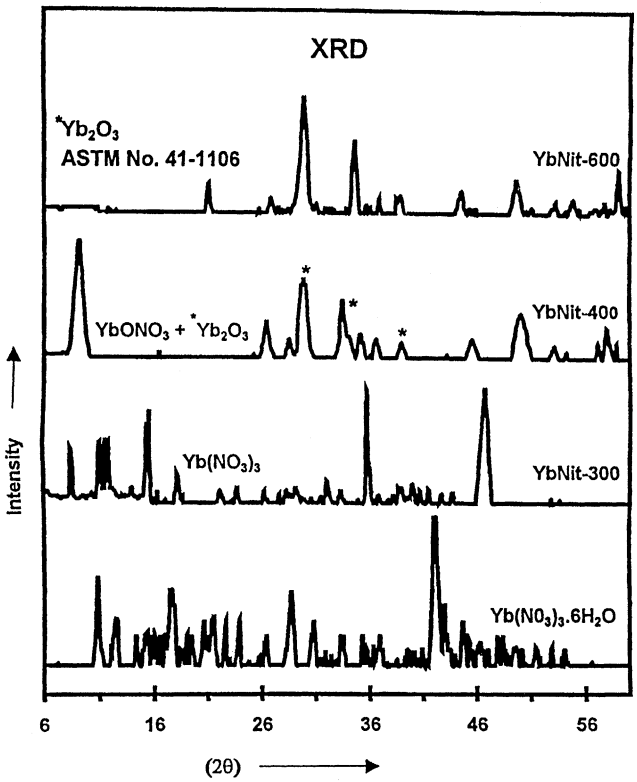

Fig. 3. X-ray powder diffractograms for the 1 h, calcination products of YbNit at the temperatures indicated.

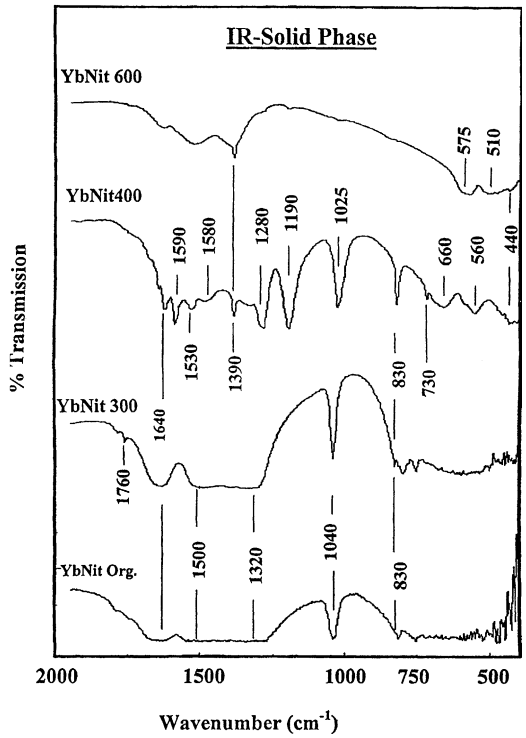

Fig. 4. IR spectra for the 1 h calcination products of YbNit at the indicated temperatures.

The formation of non-stoichiometric oxy-nitrate has been reported before [22], during the decomposition of Pr-nitrate, a different forms of $PrO_x(NO_3)_y$ was formed as an unstable intermediate which decomposed to the lower oxynitrate ($x < y$) and finally to the oxide $PrO_{1.83}$. Also, the decomposition course of Ho-nitrate pentahydrate [13] proceeded through the formation of the unstable intermediates $Ho(OH)(NO_3)_2$ and $HoO_x(NO_3)_y$ ($x > y$). The latter decomposes finally to the oxide Ho_2O_3 at 560 °C.

The mass spectra up to 450 °C (Fig. 2), detect the masses due to N_2O_5 (m/z = 108, 47, 46, 45, 32, 31, 30, 28, 16 and 14) [17]. Also, NO (m/z = 30, 16 and 15) and NO_2 (m/z = 46, 30, 16 and 15) were detected as a result of the decomposition of N_2O_5 as follows:

$$N_2O_5 \rightarrow NO + NO_2 + O_2$$

The activation energy values listed in (Table 1), for processes VIII and IX are 136 and 97 kJ/mol.

The XRD pattern of YbNit-400 (Fig. 3), displayed the pattern due to $YbONO_3$ in addition to a pattern match well with pattern (ASTM no. 41-1106) of the standard Yb_2O_3 cubic structure.

The IR spectrum (Fig. 4), of solid phase at 400 °C displays bands mainly due to nitrate [21,22]; the new bands at 1190 and 830 cm^{-1} are due to (N=O) outside of bridge and (N=O) bridge, respectively. This may suggest the formation of bridging nitrogroup. However, the evidence for the formation of oxynitrate anion $YbONO_3$, is quite convincing. Absorptions displayed between 600 and 400 cm^{-1} are related to Yb–O lattice vibrational mode [23].

Processes X and XI: Process X is strong and endothermic maximized at 470 °C. The ML determined upon completion of this process (Table 1) was 52.1% which is close to that theoretically calculated (52.03%) for the formation of the non-stoichiometric $YbO_{1.25}(NO_3)_{0.5}$. As the temperature goes up to 510 °C. The later decomposes to give the final decomposition product, Yb_2O_3, through process XI.

$$YbONO_3\ (X) \xrightarrow{470\,^\circ C} YbO_{1.25}(NO_3)_{0.5}$$

$$YbO_{1.25}(NO_3)_{0.5}\ (XI) \xrightarrow{510\,^\circ C} Yb_2O_3$$

The ML determined in this process, 57.7%, is close to that expected theoretically, 57.8%, for the over all decomposition of $Yb(NO_3)_3{\cdot}6H_2O$ into Yb_2O_3. The activation energy (ΔE) calculated for this two processes is 163 and 152 kJ/mol. These values are close to that reported for analogous compounds [13,22].

The XRD pattern at 600 °C YbNit-600 (Fig. 3), was in good agreement with both the former pattern (YbNit-400) and with that of the standard Yb_2O_3 [ASTM no. 41-1106]. Also, the IR-spectrum of the solid product at 600 °C (Fig. 4), displays only bands below 600 cm^{-1} due to Yb–O lattice vibration mode [23].

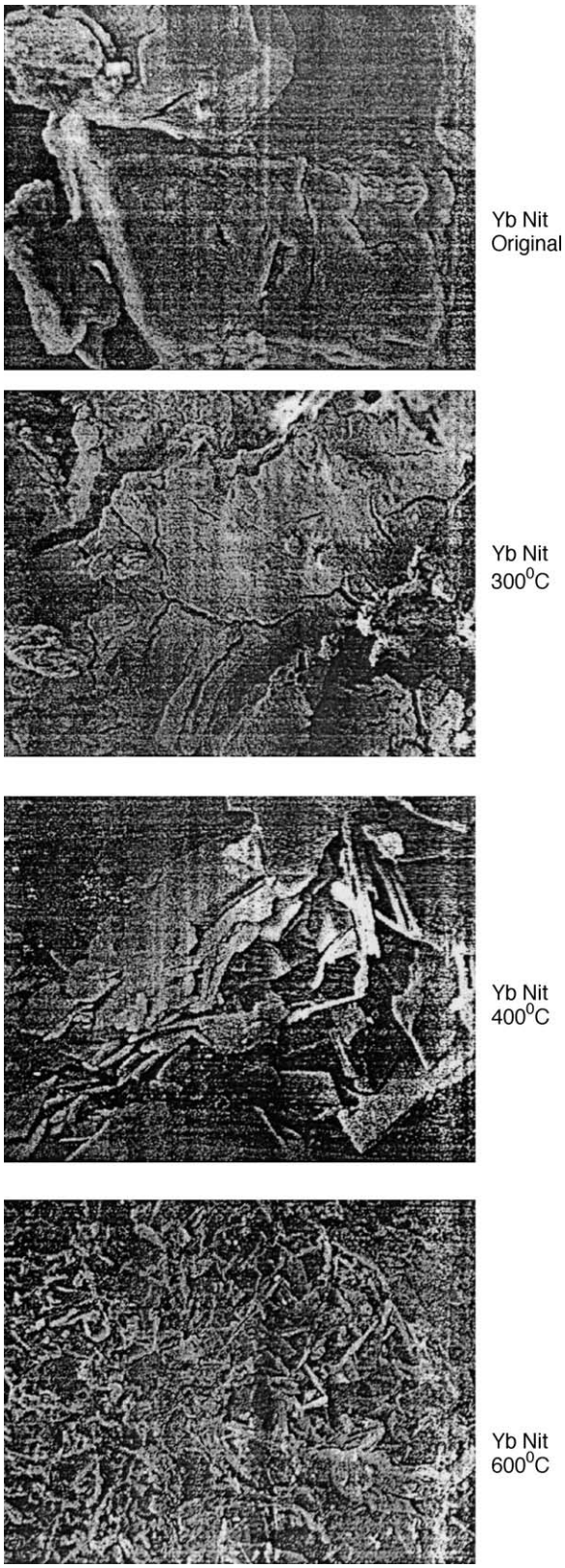

Fig. 5. Scanning electron micrograph obtained for YbNit calcined at different temperatures for 1 h (magnification 7500×).

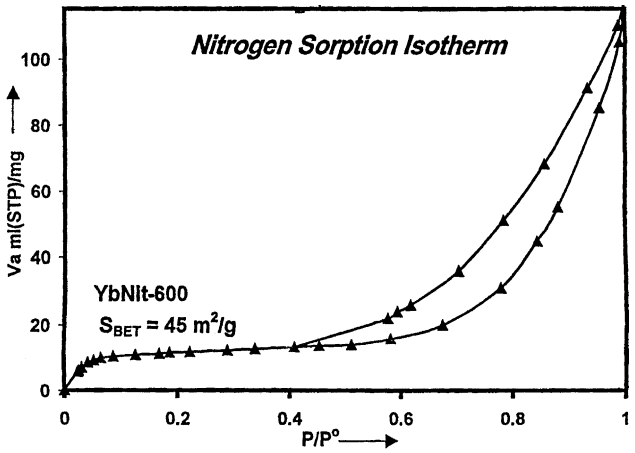

Fig. 6. Nitrogen adsorption isotherm obtained at −195 °C (using N_2 adsorption volumetric method) for YbNit-600.

3.2. Scanning electron microscopy

Attempts were made to correlate structure changes accompanying the decomposition of YbNit, with the corresponding physicochemical measurements. The SEM specimens were prepared on the basis of TG curve (Fig. 1). Original YbNit shows that the parent YbNit consists of large crystals with well defined shape (Fig. 5).

The sample heated at 300 °C (YbNit-300, Fig. 5) makes a complete change in the morphology, and the melt can be seen. Also the photo shows bubbling on the surface as a result of the evolution of water vapor as a dehydration process. In this range of temprature the TG curve (Fig. 1), indicates melting at 60 °C and dehydration at 95 °C.

When the calcination temperature goes to 400 °C, the photo shows a plate-like, irregular sheets, shape particle with a lot of cracks and small fragments arise as a consequence of the build up of the gas pressure (H_2O and HNO_3) detected by gas mass at 200 °C. At this temperature, both TG (Fig. 1) and XRD (Fig. 3), revealed the formation of $YbONO_3$.

For the 600 °C YbNit, both TG and XRD revealed the formation of Yb_2O_3. The SEM photo (YbNit-600 °C, Fig. 5) shows that the surface morphology of Yb_2O_3 is characterized by the presence of cracks, edges and voids with a rough surface. The particles are irregular sheet-shaped with different particle sizes.

3.3. Nitrogen sorption and surface area measurements

The N_2 adsorption isotherm of YbNit-600 °C is shown in (Fig. 6). The isotherm generally belongs to type IV of IUPAC classification [24]. The desorption isotherm closed at $p/p^\circ > 0.4$, which give indication the hysteresis loop is nearly of type H_3 [24]. The loop suggested that the surface pores are of slit-shaped or interplating [25]. This is in close agreement with the SEM photo of YbNit-600 (Fig. 5). The S_{BET} value determined was 45 m^2/g.

4. Conclusions

1. The thermal decomposition of hydrated YbNit in atmosphere of air involves the following path way:

$$Yb(NO_3)_3 \cdot 6H_2O \xrightarrow{\text{(II) } 95\,^\circ C} Yb(NO_3)_3{\cdot}5H_2O \xrightarrow{\text{(III) } 145\,^\circ C} Yb(NO_3)_3 \cdot 4H_2O$$

$$\xrightarrow{\text{(IV) } 165\,^\circ C} Yb(NO_3)_3 \cdot 3H_2O \xrightarrow{\text{(V) } 175\,^\circ C} Yb(NO_3)_3{\cdot}H_2O$$

$$\xrightarrow{\text{(VI) } 200\,^\circ C} Yb(NO_3)_3 \xrightarrow{\text{(VII) } 250\,^\circ C} YbO_{0.5}(NO_3)_2$$

$$\xrightarrow{\text{(VIII) } 335\,^\circ C} YbO_{0.75}(NO_3)_{1.5} \xrightarrow{\text{(IX) } 365\,^\circ C} YbONO_3$$

$$\xrightarrow{\text{(X) } 470\,^\circ C} YbO_{1.25}(NO_3)_{0.5} \xrightarrow{\text{(XI) } 510\,^\circ C} Yb_2O_3$$

2. The lower hydrate nitrate of Yb are stable but the anhydrous nitrate of Yb is unstable.
3. The non-stoichiometric forms of higher and lower oxynitrate were detected as unstable intermediates.
4. $YbONO_3$ was detected as stable and crystalline intermediate.
5. The Yb_2O_3 formed from YbNit has a large crystalline surface with different types of pores, voids and cracks and has a surface area of 45 m^2/g.
6. The gaseous decomposition products, detected by gas mass spectroscopy were H_2O vapor, HNO_3, NO, NO_2 and N_2O_5.
7. The thermal behavior of Yb-nitrate is nearly the same as other rare earth nitrate.

References

[1] P. Kofstad, Nonstoichiometry, Diffusion and Electrical Conductivity in Binary Metal Oxide, Wiley, New York, 1972, p. 289.
[2] H. Arakawa, Technol. Jpn. 21 (11) (1988) 32.
[3] K. Tanabe, K. Mismo, Y. Ono, H. Hattori, New Solid Acids and Bases Elsevier, New York, 1989, pp. 41–47.
[4] K.C. Patil, R.K. Gosavi, C.N.R. Rao, Inorg. Chem. Acta 1 (1967) 155.
[5] W.W. Wendlandt, J.L. Bear, J. Inorg. Nucl. Chem. 12 (1960) 276.
[6] D.F. Stewart, W.W. Wendlandt, J. Phys. Chem. 63 (1959) 1330.
[7] G.A.M. Hussein, Thermochim. Acta 244 (1994) 139.
[8] H.M. Ismail, G.A.M. Hussein, Powder Technol. 84 (1995) 185.
[9] G.A.M. Hussein, H.M. Ismail, Colloids Surf. 99 (1995) 129.
[10] G.A.M. Hussein, H. Korban, B. Goda, K. Miyaji, Colloids Surf. 125 (1997) 63.
[11] A.A. Balboul, G.A. Mekhemer, Colloids Surf. 125 (2001) 63.
[12] G.A.M. Hussein, J. Anal. Appl. Pyrolysis 37 (1996) 111.
[13] B.A.A. Balboul, Powder Technol. 107 (2000) 168.
[14] H.E. Kissinger, J. Anal. Chem. 29 (11) (1957) 1526.
[15] J.V. Smith (Ed.) X-ray Powder Data File, Amercain Society for Testing and Materials, Philadelphia, USA, 1960.
[16] B.C. Lippens, B.G. Linsen, J.H. de-Boer, J. Catal. 3 (1964) 32.
[17] F.W. Mclafferty, D.B. Stauffer (Eds.), The Wiley/NBS Registry of Mass Spectral Data, vol. 1, Masses from 2 to 198, New York, 1989.
[18] M.E. Brown, D. Dollimore, A.K. Galwey, Chemical Kinetics, in: C.H. Bamford, C.F.H. Tipper (Eds.), Reactions in the Solid State, vol. 22, Elsevier, Amsterdam, 1980, p. 130.

[19] G.A.M. Hussein, J. Phys. Chem. 98 (1994) 9657.
[20] K. Nakamoto, Infrared Spectra of Inorganic and Coordination Compounds, Wiley, New York, 1970, p. 253.
[21] G.A. Gadsden, Infrared Spectra of Minerals and Related Inorganic Compounds, Butterworths, London, 1975, p. 65.
[22] G.A.M. Hussein, B.A.A. Balboul, M.A.A-. Warith, A.G. Othman, Thermochim. Acta 244 (2001) 139.
[23] J.A. Goldsmith, S.D. Ross, Spectrochem. Acta (A) 23 (1967) 1909.
[24] S.J. Gregg, K.S.W. Sing, Adsorption, Surface Area and Porosity, second ed., Academic Press, London, 1982.
[25] K.S.W. Sing, Pure Appl. Chem. 54 (1982) 2201.